University of Zagreb
School of Medicine

Pia Kosanović

The connection between perineuronal nets and GABAergic interneurons in the human orbito-frontal cortex

Zagreb, 2025.

This research was done at Laboratory for immunohistochemistry at the Croatian institute for brain research, University of Zagreb School of Medicine, under the direct mentorship of Assistant professor Ivan Banovac and was submitted for evaluation for Rector's award in the academic year 2024./2025.

The research was done as part of the following research projects: "Role of proteoglycans in cortical synapse differentiation and specification of neuronal circuitries in health and perinatal hypoxia" (IP-2025-04-4135, PI: Nataša Jovanov Milošević) and "Uniqueness in development of interneurons in human prefrontal cortex during fetal life and first postnatal year – implications in pathogenesis of schizophrenia and autism" (IP-2022-10-8493, PI: Zdravko Petanjek). The part of the research pertaining to the analysis of perineuronal nets and their association with parvalbumin-expressing cells is in line with the research aims of IP-2025-04-4135, while the part of the research pertaining to the analysis of calretinin-expressing cells is in line with the research aims of IP-2022-10-8493.

LIST OF ABBREVIATIONS

BA	Brodmann area
CB	calbindin
CNS	central nervous system
CPSG	chondroitin sulfate proteoglycans
CR	calretinin
DLPFC	dorsolateral prefrontal cortex
ECM	extracellular matrix
HA	hyaluronic acid
LPCF	lateral prefrontal cortex
mPFC	medial prefrontal cortex
NDS	normal donkey serum
NeuN	neuronal nuclear antigen
oPFC	orbital prefrontal cortex
PBS	phosphate buffered saline
PFC	prefrontal cortex
PNN	perineuronal nets
PV	parvalbumin
PV^+WFA^-	PV-expressing cell not surrounded by PNN visualized using WFA
PV^+WFA^+	PV-expressing cell surrounded by PNN visualized using WFA
PV^-WFA^+	cell not expressing PV but surrounded by PNN visualized using WFA
SBA	soybean agglutinin
VVA	*Vicia villosa* agglutinin
WFA	*Wisteria floribunda* agglutinin

TABLE OF CONTENTS

1. Introduction

1.1. The prefrontal cortex

The cortex of the frontal lobe of the brain can be divided into three parts: 1) the primary motor cortex, 2) the premotor cortex and 3) the prefrontal cortex (PFC), which is the largest of the three. The PFC is also known as the granular frontal cortex since it typically has an internal granular layer (IV) (Fuster, 1988). Nowadays, the PFC is usually defined as the part of the cerebral cortex receiving inputs from the mediodorsal thalamic nucleus. The PFC is further divided into two parts: the lateral PFC (LPFC) and ventromedial PFC (vmPFC). The ventral portion of the vmPFC is also commonly referred to as the orbitofrontal PFC (OFC). The LPFC can be subdivided into the dorsolateral PFC (DLPFC) and the ventrolateral PFC (VLPFC) (Fuster, 2008). The PFC is involved in higher order cognitive functions and allows integration of information from different associative cortical regions. Because of its many connections to regions that regulate the productions of mood-altering neurotransmitters, the PFC is also thought to have an impact on the emotional state of humans (Hathaway and Newton, 2025). The OFC is a region of the PFC that, in primates, occupies the ventral surface of the frontal lobe (Kringelbach and Rolls, 2004). The OFC is involved in integration of internal and external information, visceral sensations, the sense of smell, emotional regulation and magnitude of reward (Mitchell and Beech, 2011).

Cytoarchitecture describes the distribution of different neuronal cell types, arrangement of cells in horizontal layers and vertical columns as well as cortical thickness (Zilles, Palomero-Gallagher and Amunts, 2015). The most widely used cytoarchitectonic maps are those devised by Korbinian Brodmann (Brodmann, 2005; Mauguière, Frot and Isnard, 2008). The vmPFC includes areas 11, 13, 14 in the ventral part and areas 12, 24, 25, 32 and 33 in the medial part. The LPFC includes areas 8, 9, 10 and 46 in the dorsolateral and 44, 45 and 47 in the ventrolateral part (Fuster, 2008).

The cerebral cortex can be divided into different regions based on the thickness of different types of cortical layers (granule and pyramidal cells) and the number of layers. The PFC typically has six distinct layers (I-VI) (Mauguière, Frot and Isnard, 2008).

1.2. GABAergic interneurons

GABAergic interneurons are the main source of inhibition in the mammalian brain. They constitute 10% – 25% of the total number of cortical neurons and are diverse in their morphology and functional properties (Le Magueresse and Monyer, 2013). The PFC contains a heterogenous population of neurons, including GABAergic inhibitory interneurons. There are many different subtypes of cortical GABAergic interneurons that can be identified by expression of specific molecular markers. Two of the most numerous interneuron populations in the human cortex express calretinin (CR) and parvalbumin (PV), which are both calcium binding protein

1.3. Perineuronal nets (PNNs)

Perineural nets (PNNs) are structures that surround the cell body and cellular processes of neurons. PNNs containing N-acetylgalactosamine are found both surrounding excitatory pyramidal neurons and certain populations of GABAergic neurons, primarily PV-expressing (PV^+) neurons, while CR-expressing (CR^+) neurons are not surrounded by such PNNs. PNNs are a type of condensed extracellular matrix (ECM) and are formed by chondroitin sulfate proteoglycans, hyaluronic acid, link proteins and glycoproteins (e.g. tenascin-R) (Mauney *et al.*, 2013).

PNNs are involved in fast-spiking firing by buffering cations and by regulating synaptic plasticity, they play an important role in maintaining the integrity of cortical microcircuitry (Mauney *et al.*, 2013).

PNNs are present throughout the CNS and are unevenly distributed in different brain regions. (Karetko and Skangiel-Kramska, 2009). PNNs are observed surrounding nerve cells in the substantia nigra, hippocampus, spinal cord, deep nuclei of the cerebellum, visual cortex and the somatosensory cortex (Kwok *et al.*, 2011). PNNs encircle projection neurons in the brain stem, spinal cord, and deep cerebral nuclei (Karetko and Skangiel-Kramska, 2009).

Methods of visualizing PNNs include various staining methods: (1) lectins like *Wisteria floribunda* agglutinin (WFA), *Vicia villosa* agglutinin (VVA) and soybean agglutinin (SBA); (2) proteoglycans that are sulfate conjugates and can be detected using iron colloid; (3) Kopsh's silver nitrate or methylene blue that visualizes core proteins or proteoglycans. Immunohistochemical staining methods are widely used for the detection of core proteins (Karetko and Skangiel-Kramska, 2009).

2. Hypothesis and research aims

The hypothesis of this research was that there are differences in the proportion, laminar distribution of perineuronal nets and GABAergic interneurons within the human orbitofrontal cortex between Brodmann area 10 (BA10m) and Brodmann area 13 (BA13b).

The main aim of the research was to determine the proportion of PNNs and GABAergic interneurons in BA10m and BA13b.

The specific aims of the research were:

1) to determine the distribution of PNNs and GABAergic interneurons across all layers in BA10m and BA13b;
2) to determine the relative proportion of PV^+ cells surrounded by PNNs;
3) to determine the morphological characteristics of different GABAergic interneuron populations and the associated PNNs.

3. Materials and methods

3.1. Specimen collection and tissue preparation

The brain samples used in this research originate from blocks of archived tissue of the prefrontal cortex from six different brains that are a part of the Zagreb neuro-embryological collection (Kostovic *et al.*, 1991; Judaš *et al.*, 2011). The tissue used was previously stored postmortem material taken exclusively from regularly performed autopsies and coded with appropriate identifiers. The data on sex, age and cause of death of the individual from which the sample originated are sorted in a separate protocol. The individuals from whom the brain tissue was taken had no history of psychological or neurological diseases and during the autopsy no neuropathological abnormalities were observed. No pre-agonal state was noted before death, and therefore the postmortem interval represents the actual time elapsed since the death of the neuronal cells.

Table 1. Brain tissue samples used in the study.

Brain	Sex	Age (years)	Postmortem interval (hours)	Cause of death
ČO382	M	40	6,5	Sudden cardiac death
ČO383	M	51	11	Sudden cardiac death
ČO384	M	46	6	Sudden cardiac death
ČO385	M	29	8	Polytrauma
ČO386	M	37	6	Sudden cardiac death
ČO387	M	44	6	Methadone/benzodiazepine overdose

The brains were cut into blocks of tissue and were then fixed by immersion in 4% formaldehyde, cryoprotected in 10% and 20% sucrose solution and then frozen and stored at a temperature of -80°C. A portion of the tissue samples were subsequently thawed and embedded in paraffin blocks (Sadeghipour and Babaheidarian, 2019). The paraffin blocks were then cut using a microtome (LEICA HI1210) into 20 μm thick slices (Sy and Ang, 2019), and placed on VitroGnost Plus Ultra adhesive glass slides (Biognost, Croatia).

In this study two areas of the PFC were analyzed: BA10m and BA13b. BA10m is found along the medial frontal surface. On the frontal section of the gyrus rectus, it lies just medially to BA14r (Figure 1). BA13b occupies the medial bank of the olfactory sulcus rostral to 13a, and lies just laterally to area 14r on the frontal section of the gyrus rectus (Öngür, Ferry and Price, 2003). For each brain, a total of six histological slides (three per staining type) were analyzed from each Brodmann area.

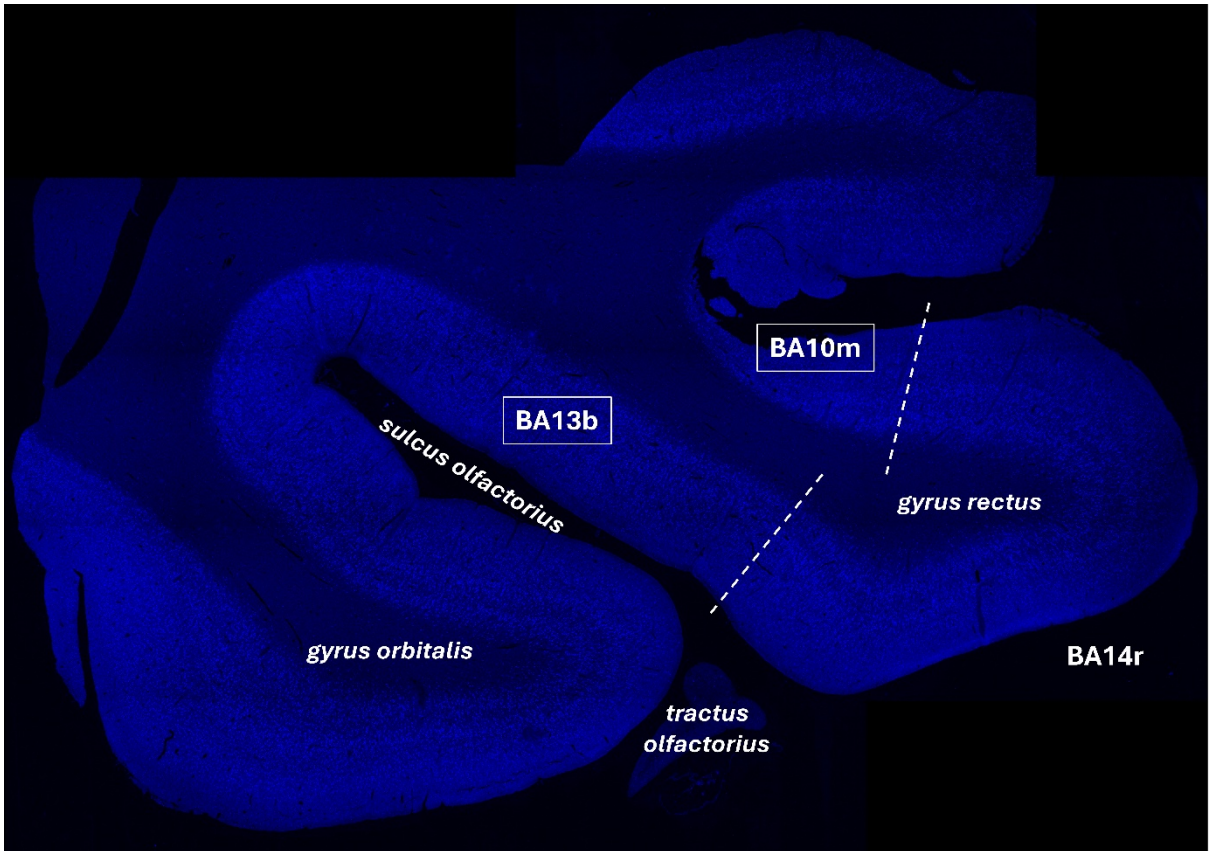

Figure 1. Frontal section of OFC showing the location of BA10m and BA13b.

3.2. Immunohistochemical analysis

Indirect immunofluorescence was used to analyze histological sections of the cerebral cortex, in which primary antibodies bind to target molecules, while the fluorophore-labeled secondary antibody recognizes and binds to the Fc-fragment of the primary antibody (Betterle and Zanchetta, 2012). The primary antibody targeting the neuronal nuclear antigen (NeuN) was used to visualize cortical neurons. To visualize cortical GABAergic interneurons, antibodies against the calcium-binding proteins PV and CR were used. PNNs were detected using fluorescently labeled WFA.

The immunohistochemical staining procedure followed established protocols for paraffin-embedded tissue sections (Banovac *et al.*, 2019, 2022; Zaqout, Becker and Kaindl, 2020). The tissue sections were first exposed to a strong light source for 48 hours to minimize lipofuscin-related autofluorescence(Neumann and Gabel, 2002; Sun, Ip and Chakrabartty, 2017). Following light exposure, sections were deparaffinized by two 10-minute immersions in xylene, then rehydrated through a descending ethanol series: two immersions in 100% ethanol, one in 96%, and one in 70%, each for 5 minutes.

The sections were then rinsed in phosphate buffered saline (PBS, pH 7.4), followed by antigen retrieval using a citrate buffer at pH 6.0 (Boenisch, 2005). After additional rinsing in PBS, the tissue was encircled with a hydrophobic barrier. To reduce non-specific binding of secondary antibodies, protein

blocking was performed for one hour using a blocking solution made of normal donkey serum (NDS; Chemicon, USA) diluted 1:30 in permeabilization solution (0.3% Triton X-100; Sigma-Aldrich, USA).

After blocking, sections were incubated for 24 hours at 4°C with NDS and a primary antibody solution containing an anti-NeuN (rabbit, polyclonal, abcam, UK; cat. no. ab104225, lot: GR3370892-1) antibody in combination with either an anti-PV antibody (rabbit, polyclonal, abcam, UK; cat. no. ab11427, lot: GR3317380-2) and WFA conjugated with fluorescein (Vector Laboratories, USA; cat. no. FL-1351, lot: ZG0903) or an anti-CR antibody (mouse, monoclonal, Swant, Switzerland, cat. no. 6B3, lot: 010399).

Following primary antibody incubation, sections were rinsed in PBS and then incubated for two hours with highly cross-adsorbed donkey secondary antibodies: conjugated anti-mouse Alexa 488 (ThermoFisher, USA, cat. no. A21202, lot: 2428531) and conjugated anti-rabbit Alexa Fluor 546 (ThermoFisher, USA; cat. no. A10040, lot: 2128963). Subsequently, sections were exposed for one minute to TrueBlack Lipofuscin Autofluorescence Quencher (Biotium, USA) to minimize lipofuscin and background autofluorescence. After a final PBS rinse, samples were coverslipped using VectaMount® AQ Aqueous Mounting Medium (Vector Laboratories, USA) and stored at +4°C.

3.3. Processing and quantitative analysis of histological slides

Staining on histological slides was visualized using a laser scanning confocal microscope (Olympus FLUOVIEW FV3000RS, Japan) located in the Laboratory for confocal microscopy at the Croatian Institute for Brain Research (CIBR), University of Zagreb School of Medicine. This confocal system enables high-resolution imaging across multiple optical planes and allows simultaneous visualization of different fluorescent labels. Entire regions of interest were captured at 20x magnification, covering 20 to 30 visual fields per section. In each visual field, five planes spanning the full section thickness were recorded at 4 μm intervals, with a resolution of 1024x1024 pixels. The resulting image had a spatial resolution where one pixel corresponded to 0.6215 μm (Banovac *et al.*, 2022).

Image processing was carried out using Neurolucida 2020 software (MBF Bioscience, Vermont, USA) within the NeuroMorphometry Laboratory at CIBR. For each section, the counting column specific to the respective Brodmann area was defined, in which neurons and PNNs were analyzed. The counting columns were drawn to be 1000 μm wide at the pial surface and oriented perpendicular to cortical layers, following the general orientation of neuronal structures. Each column was subdivided into separate contours representing individual cortical layers.

Each molecular marker (NeuN, PV, CR and WFA) was assigned a distinct marker in Neurolucida. To identify neurons, the software's "Detect Cells" function was used, which employs an image-processing algorithm to automatically locate neuronal cell bodies in confocal images. This function required defining regions of interest (the outlined counting columns), and setting both minimum and maximum cell diameters as well as an intensity threshold to distinguish the signal from background. Once the

software placed markers for identified neurons, each column was manually reviewed to correct misidentified cells (Banovac *et al.*, 2022). Because the software algorithm is not optimized for detecting PNNs, the quantification of PNNs was done completely manually. After marking PV and WFA signals, colocalization was defined by setting a maximum distance criterion between two markers at 10 μm, corresponding to the average soma diameter of cortical interneurons, to determine whether two signals belonged to the same cell. The software automatically applied a colocalization marker when this criterion was met. All such markers were subsequently verified by manual inspection.

The neuron cell bodies were reconstructed using Neurolucida 2020 (MBF, Vermont, USA) based on the following principles: the cell body contour was drawn along the very edge of the cell body and the cellular processes were not encompassed by the cell body contour. Only cell bodies that could be clearly delineated from the background were chosen for reconstruction. A total of 1512 cell bodies were reconstructed in this way (1101 CR^+ cell bodies and 341 PV^+ or WFA^+ cell bodies). The following morphometric parameters were analyzed for each cell: soma surface (*Area*), ratio between the larges and smallest diameter of the soma contour (*Aspect ratio*), and the complexity/irregularity of the soma circumference (*Form Factor*) (Prkačin, Petanjek and Banovac, 2024).

3.4. Statistical analysis

All statistical analyses were conducted using GraphPad Prism software, version 10.5.0 (GraphPad Software, La Jolla, USA).

To evaluate the proportions of PV^+ neurons and PNNs relative to the total number of neurons, the mean values across all brains were calculated for each cortical layer within both Brodmann areas as well as for all cortical layers combined within each region. The results were presented as mean ± standard deviation. In order to assess differences in the proportion of PNNs and GABAergic neurons between BA10m and BA13b, the paired t-test was used, treating data from the same brain as paired samples.

Morphometric parameters were presented as median with interquartile range (IQR) and visualized using box and whiskers plots. For comparison of morphometric parameters between different cell types, the Mann-Whitney test (for single comparisons) or Kruskal-Wallis test (for multiple comparisons) were used because most morphometric data are sampled from non-normal distributions.

A *p*-value of less than 0.05 was considered statistically significant for all analyses. Differences in total PNN proportions, the connection of PNNs and GABAergic interneurons, as well as variations across layers were visualized using estimation plots.

The relative proportions of the following cells were also calculated: PV^+ cells surrounded by WFA^+ PNNs (PV^+WFA^+ cells), PV^+ cells not surrounded by WFA^+ PNNs (PV^+WFA^- cells, and PV^- cells surrounded by WFA^+ PNNs (PV^-WFA^+ cells). These relative proportions were visualized using bar graphs.

4. Results

4.1. Interneuron proportion and surface density in Brodmann areas 10m and 13b

4.1.1. Proportion and surface density of parvalbumin-expressing interneurons

Quantitative analysis of the proportion of PV^+ cells relative to the overall neuronal population ($NeuN^+$ cells) was performed across all six cortical layers in both BA10m and BA13b. Overall, the mean PV/NeuN ratios had rather similar values in both regions: 5.05% in BA10m vs. 4.99% in BA13b, with no statistically significant difference (paired t-test, p = 0.9273;). Quantification of PV^+ interneuron surface density revealed no statistically significant differences between BA10m and BA13b. BA10m exhibited a slightly higher mean PV^+ density (282.1 vs. 227.0 cells/mm²), but this difference was not statistically significant (p = 0.4601; Figure 2).

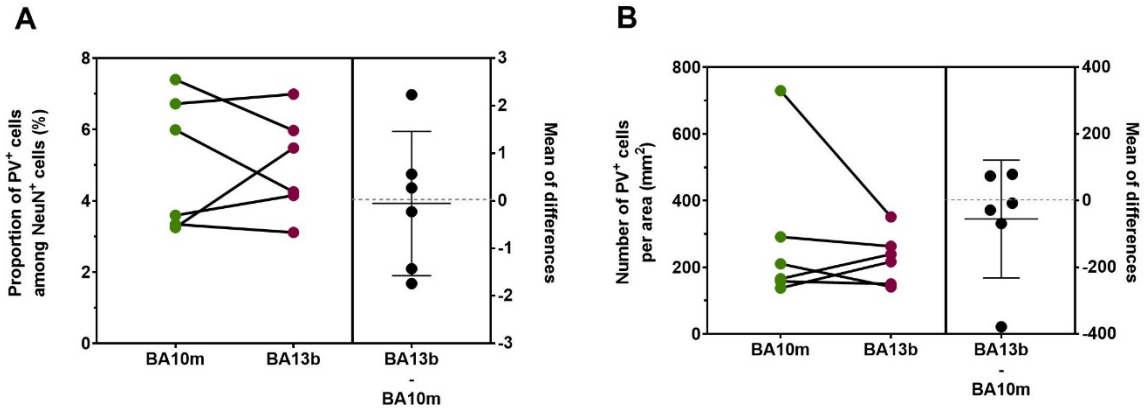

Figure 2. Estimation plots showing the comparison in the amount of PV^+ neurons between BA10m and BA13b. (**A**) Proportion of PV^+ cells among $NeuN^+$ cells across all cortical layers. (**B**) Surface density of PV^+ cells across all cortical layers.

Interestingly, layer V exhibited the largest inter-regional difference in the proportion of PV^+ cells: 4.33% in BA10m vs. 5.54% in BA13b (mean difference = 1.20%) although this difference was not statistically significant (p = 0.1131). Layer IV had the highest proportion of PV^+ cells in both cortical regions – 7.72% in BA10m, and 7.45% in BA13b. Laminar analysis of surface density showed that the interregional difference in density of PV^+ cells was once again the highest in layer V (mean difference = 11.31 cells/mm², in favor of BA13b, p = 0.2519).

4.1.2. Proportion and surface density of calretinin-expressing interneurons

Quantitative analysis of the proportion of CR^+ cells relative to $NeuN^+$ cells revealed no statistically significant differences between BA10m and BA13b (Figure 3). The mean proportions of CR^+ cells were nearly identical (BA10m: 9.02 ± 3.62; BA13b: 8.95 ± 2.68) and the difference was not statistically significant (paired t-test, p = 0.9456). Similarly, comparisons within individual cortical layers revealed

no significant differences ($p > 0.05$ for all layers). The highest overall CR^+ cell proportion was observed in layer I of both BA10m (36.68 ± 20.52%) and BA13b (33.21 ± 9.49%), and the largest interregional difference was also found in this layer (mean difference = 3.48%, $p = 0.6489$; Figure 4).

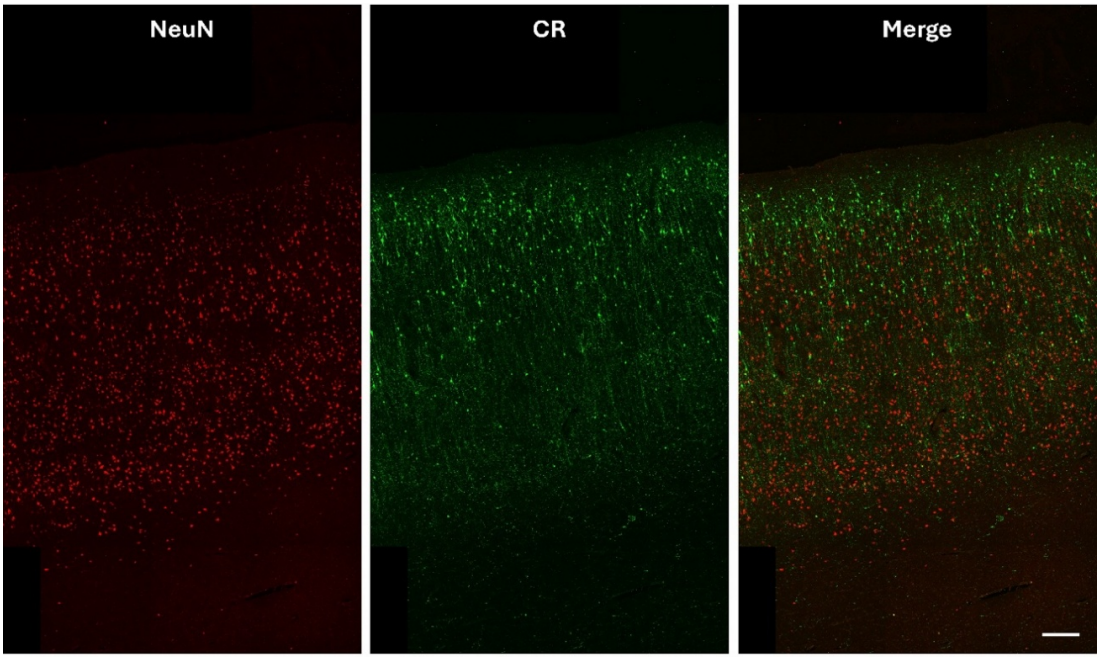

Figure 3. Representative images showing the laminar distribution of $NeuN^+$ cells (red) and CR^+ cells (green) in BA10m. Scale bar: 200 µm.

No significant differences were found in CR^+ cell surface density between BA10m and BA13b, either overall ($p = 0.2781$) or within individual layers ($p > 0.05$ for all layers). The overall mean difference was 40.89 cells/mm². The largest mean difference was observed in layer II (13.79 cell/mm^2), followed by layers IV (12.60 cell/mm^2) and I (11.52 cell/mm^2). Layers V and VI showed minimal interregional differences and the highest CR^+ cell density was observed in layer 2 in both regions.

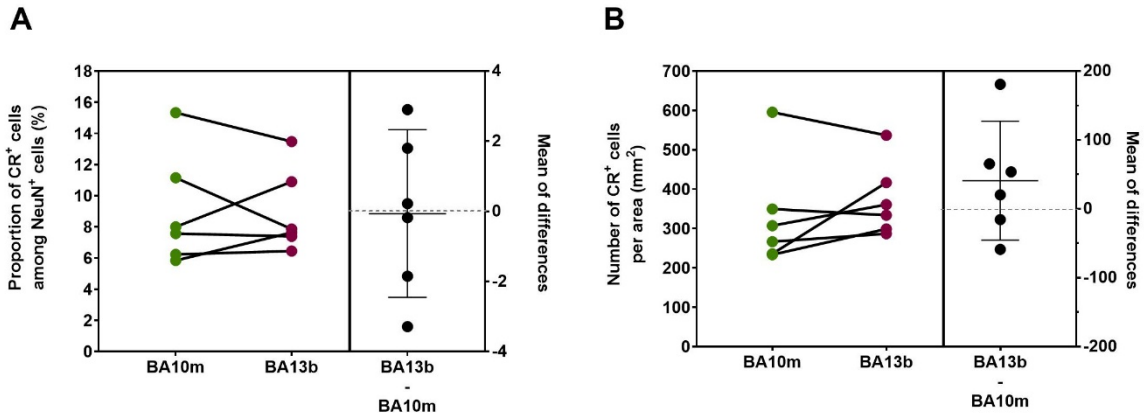

Figure 4. Estimation plots showing the comparison in the amount of CR^+ neurons between BA10m and BA13b. (**A**) Proportion of CR^+ cells among $NeuN^+$ cells across all cortical layers. (**B**) Surface density of CR^+ cells across all cortical layers.

4.2. Proportion and surface density of perineuronal nets in Brodmann areas 10m and 13b

Quantitative analysis of the proportion of WFA^+ PNNs surrounding $NeuN^+$ cells revealed no statistically significant differences between BA10m and BA13b, neither in laminar distribution nor in total values (Figure 5). The proportion of WFA^+ PNNs was, on average, higher in BA13b in all layers, except in layer II. Layer-specific comparisons showed that the highest mean difference was observed in layer 5 (1.11%), followed by layer 3 (1.05%), but remained non-significant (p = 0.1185 and p = 0.1325, respectively). The highest proportions of WFA^+ PNNs were observed in both regions in layers III (5.90% in BA10m, 6.95% in BA13b) and IV (5.90% in BA10m, 6.40% in BA13b).

When all layers were combined, the total proportion of WFA^+ PNNs was slightly higher in BA13b (4.83%) than in BA10m (4.19%) (paired t- test, p = 0.2446). These results indicate that, while BA13b shows a consistent trend of higher proportions of WFA^+ PNNs across multiple cortical layers, the differences were subtle and not statistically significant.

Quantitative analysis of the surface density of WFA^+ PNNs revealed no statistically significant differences between the regions BA10m and BA13b ($p > 0.05$ for all cortical layers).

Layer III showed a considerable but non-significant decrease in WFA^+ PNN density in BA13b relative to BA10m (mean difference = 54.52/mm², p = 0.41), while layer IV displayed the opposite trend, with higher values in BA13b (mean difference = 16.28/mm², p = 0.44). The highest density of WFA^+ PNNs was observed in layers III and IV in both regions. Overall WFA^+ PNN density per area was slightly lower in BA13b (191.3 PNNs/mm^2) compared to BA10m (215.5 PNNs/mm^2), but this difference was also not significant (p = 0.71;).

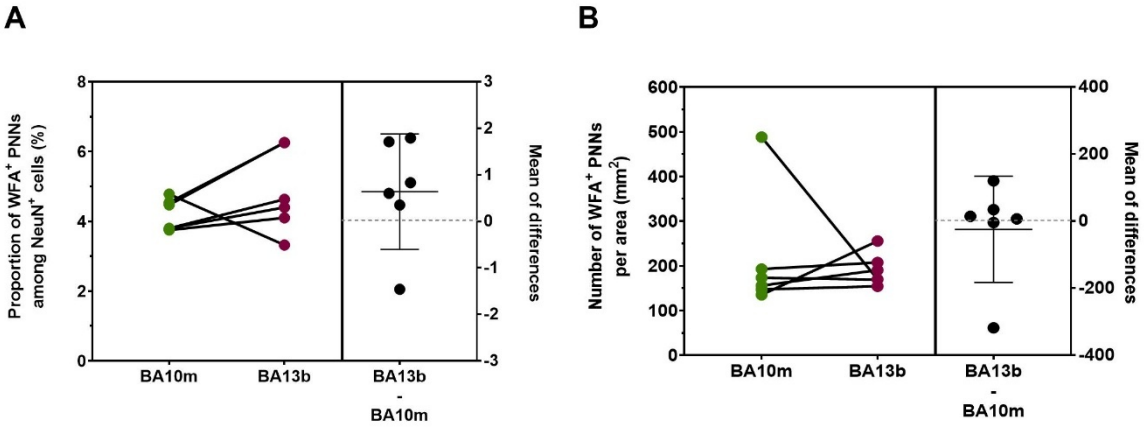

Figure 5. Estimation plots showing the comparison in the amount of WFA^+ PNNs between BA10m and BA13b. (**A**) Proportion of WFA^+ PNNs among $NeuN^+$ cells across all cortical layers. (**B**) Surface density of WFA^+ PNNs across all cortical layers.

4.3. Relationship between parvalbumin-expressing interneurons and perineuronal nets

4.3.1. Parvalbumin-expressing neurons surrounded by perineuronal nets

The proportion of PV^+WFA^+ (Figure 6) cells relative to the total neuronal population was very similar in the two analyzed cortical regions (BA10m: 2.31%; BA13b: 2.24%), and the difference was not significant (paired t-test, $p = 0.8345$; Figure 7). The highest proportion of PV^+WFA^+ cells was found in layer IV in both regions (BA10m: 3.74%; BA13b: 3.67%), while layer III contained the second-highest proportion of PV^+WFA^+ cells (BA10m: 2.98%; BA13b: 3.08%). The interregional differences across all cortical layers were also not statistically significant ($p > 0.05$ for all layers).

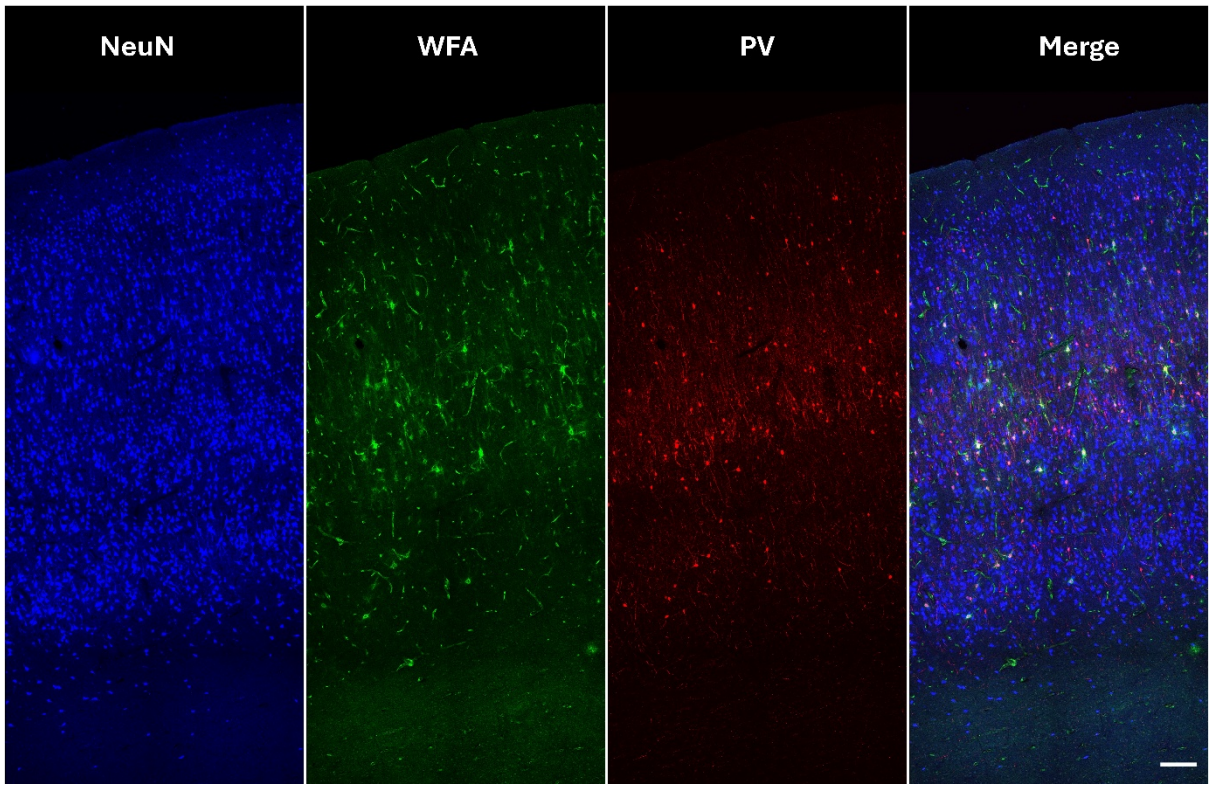

Figure 6. Representative images showing the laminar distribution of $NeuN^+$ cells (blue), WFA^+ PNNs (green), and PV^+ cells (red) in BA10m. Scale bar: 200 µm.

The average surface density of PV^+WFA^+ cells also did not differ significantly between BA10m and BA13b (mean difference = 31.07; $p = 0.4455$), and the same was true for all individual layers ($p > 0.05$ for all layers). The largest mean difference (40.35 cells/mm^2) was found in layer III, suggesting a higher PV^+WFA^+ cell density in BA10m compared to BA13b, though still not statistically significant ($p = 0.3661$). The highest surface density in BA10m was found in layer III with 60.83 cells/mm^2 and for BA13b the highest surface density was observed in layer IV with 44.41 cells/mm^2.

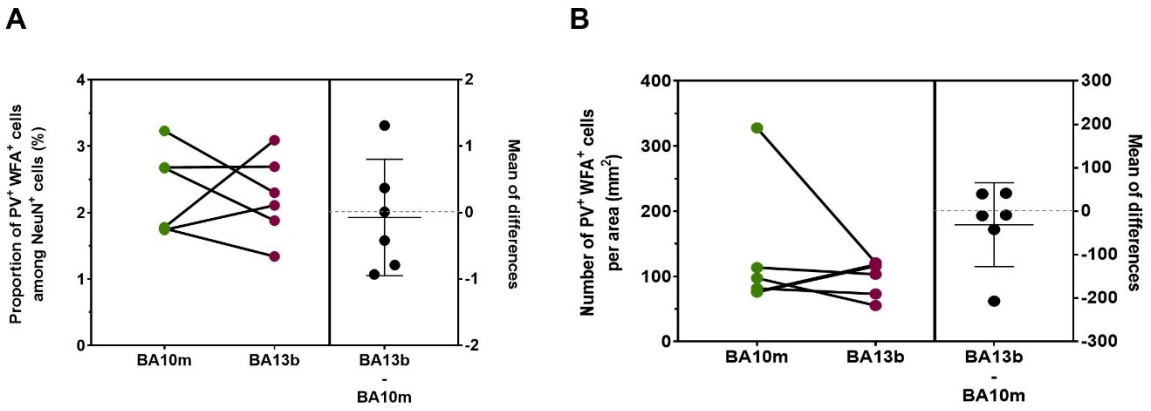

Figure 7. Estimation plots showing the comparison in the amount of PV^+WFA^+ cells between BA10m and BA13b. (**A**) Proportion of PV^+WFA^+ cells among $NeuN^+$ cells across all cortical layers. (**B**) Surface density of PV^+WFA^+ cells across all cortical layers.

4.3.2. Relative proportions of PV^+WFA^-, PV^+WFA^+, and PV^-WFA^+ cells

The overall proportion of PV^+ cells and WFA^+ PNNs (Figure 8) in layer I was very low – both PV^+ cells and WFA^+ PNNs were only sporadically present in this layer, making informative comparisons between cortical regions relatively difficult. In the other cortical layers, the number of both PV^+ cells and WFA^+ PNNs was sufficient to compare the relative proportions of PV^+WFA^-, PV^+WFA^+, and PV^-WFA^+ cells between BA10m and BA13b.

In layer II, BA10m showed the highest proportion of PV^+WFA^- cells (63.93%), followed by PV^-WFA^+ (19.67%) and PV^+WFA^+ (16.39%). In contrast, BA13b displayed an even higher prevalence of PV^+WFA^- cells (75.32%), with lower proportions of PV^+WFA^+ (14.29%) and PV^-WFA^+ (10.39%) cells.

In layer III, BA10m showed a relatively balanced distribution among PV^+WFA^- (38.30%), PV^+WFA^+ (31.45%), and PV^-WFA^+ (30.25%) cells. In contrast, BA13b presented a lower proportion of PV^+WFA^- cells (32.52%) and a higher proportion of PV^-WFA^+ cells (37.99%), with PV^+WFA^+ cells accounting for 29.49%.

In layer IV, BA10m had the following relative proportions: 41.86% for PV^+WFA^-, 37.21% for PV^+WFA^+, and 20.93% for PV^-WFA^+ cells. In comparison, BA13b had a slightly more even distribution: 36.10% for PV^+WFA^-, 35.61% for PV^+WFA^+, and 28.29% for PV^-WFA^+ cells.

In layer V, BA13b had higher proportions of PV^+WFA^- (38.31%) and PV^-WFA^+ (35.07%) cells compared to BA10m (31.89% and 28.74%, respectively). However, PV^+WFA^+ cells were more abundant in BA10m (39.37%) than in BA13b (26.62%), suggesting that in BA10m, PV^+ interneurons are more frequently surrounded by PNNs.

In layer VI, BA10m showed 45.39% $PV^{+}WFA^{-}$, 36.17% $PV^{+}WFA^{+}$, and 18.44% $PV^{-}WFA^{+}$ cells. BA13b had lower proportions of $PV^{+}WFA^{-}$ (36.60%) and $PV^{+}WFA^{+}$ cells (33.51%), but a higher proportion of $PV^{-}WFA^{+}$ cells (29.90%).

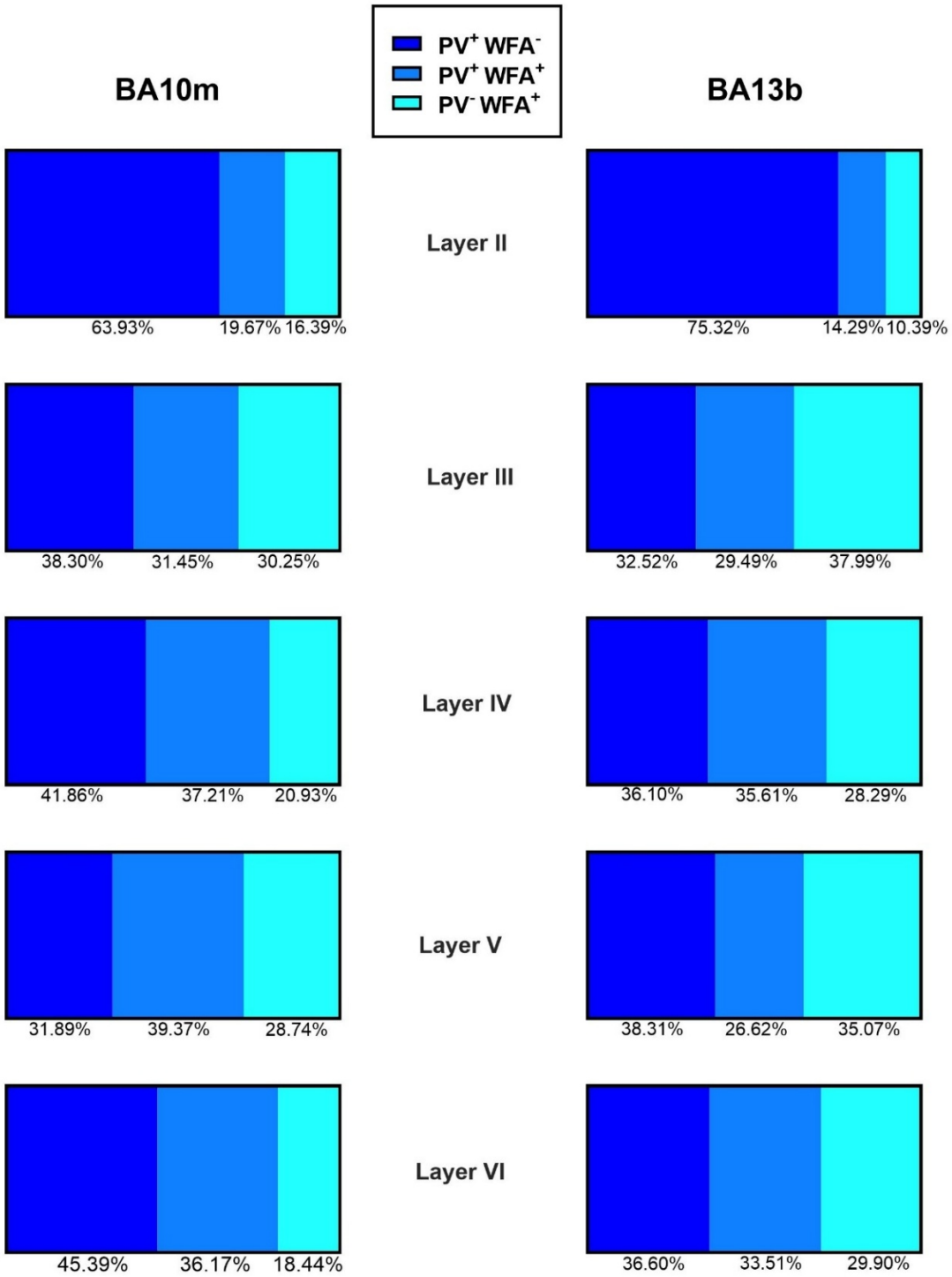

Figure 8. Distribution of $PV^{+}WFA^{-}$, $PV^{+}WFA^{+}$, and $PV^{-}WFA^{+}$ cells in cortical layers II – VI in BA10m and BA13b. Percentages indicate the relative proportion of each cell type within a given layer.

This analysis revealed that the most prominent interregional differences in the composition of PV+ cells and WFA+ PNNs were present in layers II and VI. Interregional differences in layers III and V were more subtle, while differences in layer IV were the least prominent.

A comparative analysis of cell populations in all layers (Figure 9) in BA10m and BA13b revealed similar proportions of PV^+WFA^- cells (39.74% and 36.81%, respectively). There was a slightly higher percentage of PV^-WFA^+ cells observed in BA13b (33.84%) compared to BA10m (26.75%), while the proportion of PV^+WFA^+ cells was slightly higher in BA10m (33.50%) than in BA13b (29.35%).

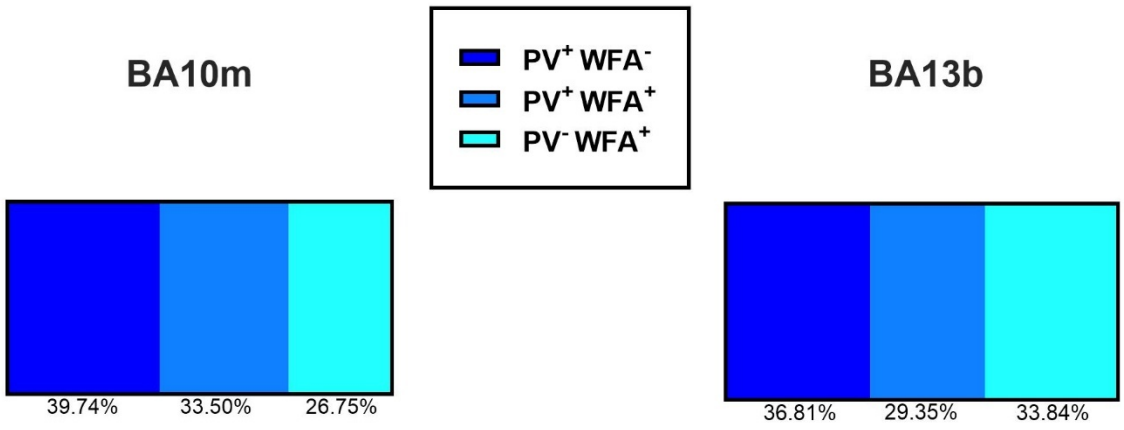

Figure 9. Relative proportions of PV^+WFA^-, PV^+WFA^+, and PV^-WFA^+ cells across all cortical layers in BA10m and BA13b.

4.4. Morphological characteristics of GABAergic interneurons and perineuronal nets

4.4.1. Comparison of morphological characteristics of GABAergic interneurons

Morphometric analysis revealed that PV^+ cells in BA10m had significantly larger somas compared to CR^+ cells (Mann Whitney test, $p < 0.0001$). The median area was 120.6 µm² (IQR: 93.83 – 164.3 µm²) for PV^+ cells and 78.90 µm² (IQR: 61.34 – 100.6 µm²) for CR^+ cells. In contrast, no significant differences were observed for aspect ratio ($p = 0.1665$) or form factor ($p = 0.2267$) between the two cell populations in BA10m. These findings indicate that while PV^+ neurons exhibit significantly larger somatic size, while their elongation and shape regularity were comparable to CR^+ neurons in BA10m (Figure 10). In BA13b, PV^+ neurons displayed significantly larger somatic areas compared to CR^+ neurons ($p < 0.0001$). The median soma area of PV^+ cells in BA13b was 121.8 µm² (IQR: 96.76 – 147.2 µm²) while that of CR^+ cells was 85.9 µm² (IQR: 66.63 – 112.7 µm²). Moreover, aspect ratio differed significantly between groups ($p < 0.0001$), with CR^+ neurons exhibiting more elongated cell bodies (1.48, IQR: 1.33 – 1.71) relative to PV^+WFA^- neurons (1.37, IQR: 1.26 – 1.59). Form factor was also significantly different ($p = 0.0013$) with PV^+ neurons showing more regular cell contours (0.89, IQR: 0.85 – 0.92) than CR^+ neurons (0.87, IQR: 0.82 – 0.91) (Figure 11).

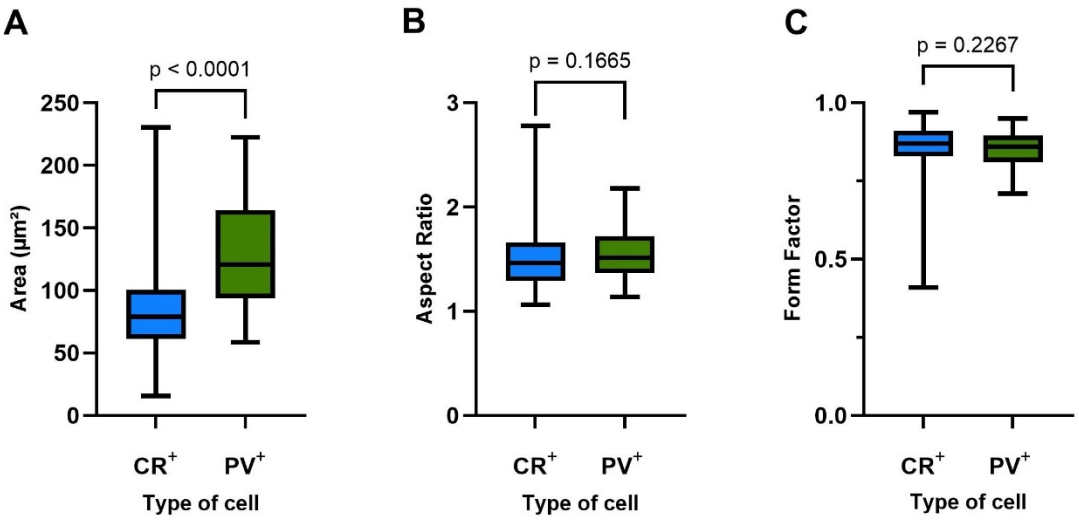

Figure 10. Morphometric comparison of CR^+ and PV^+ cells in BA10m. Box plots display differences in (**A**) soma area (µm²), (**B**) aspect ratio, and (**C**) form factor between CR^+ and PV^+ neurons.

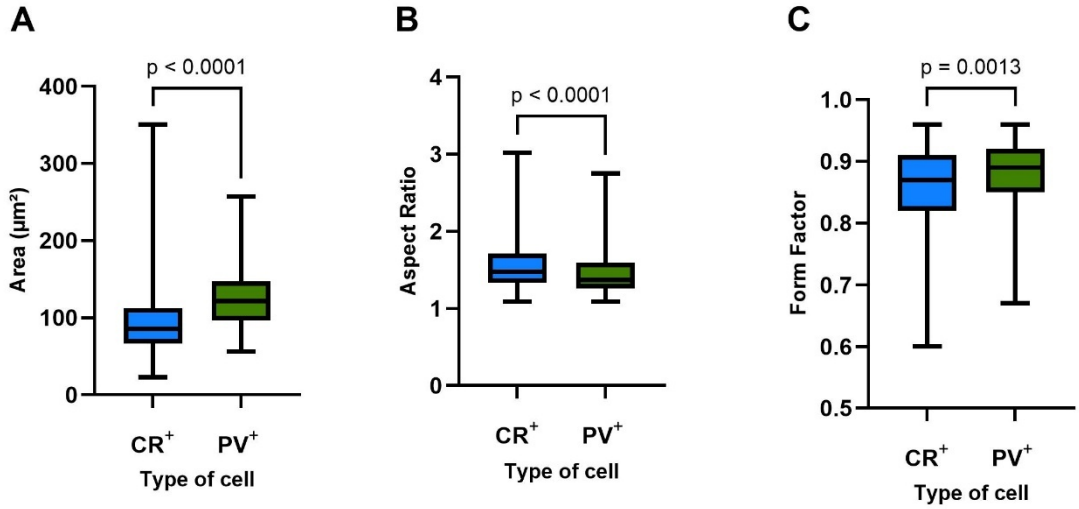

Figure 11. Morphometric comparison of CR^+ and PV^+ cells in BA13b. Bar graphs display differences in (A) cell area (µm²), (B) aspect ratio, and (C) form factor between CR^+ and PV^+ neurons.

Morphological profiling of interneurons revealed both shared and region-specific features across BA10m and BA13b. In both regions, PV^+ neurons exhibited significantly larger somatic areas than CR^+ neurons, highlighting a consistent size-based distinction between these interneuron subtypes. However, in BA13b aspect ratio and form factor also significantly differ between PV^+ and CR^+ cells, with CR^+ neurons showing more elongated and less circular profiles, suggesting greater structural divergence between these cell types in BA13b.

Overall, BA13b displayed greater morphological heterogeneity and shape-related differentiation among interneuron subtypes compared to BA10m, potentially reflecting differences in microcircuit specialization between these cortical areas.

4.4.2. Comparison of morphological characteristic of PV^+WFA^-, PV^+WFA^+ and PV^-WFA^+ cells

For the comparison between PV^+WFA^-, PV^+WFA^+ and PV^-WFA^+ cells there were no observed significant differences in the analyzed morphometric parameters between BA10m and BA13b. Therefore, the data for this morphometric analysis are pooled from both cortical regions.

The soma area was significantly different between all three analyzed cell groups (Kruskal-Wallis test, $p < 0.0001$), with PV^-WFA^+ cells showing the largest median area, followed by PV^+WFA^+, and then PV^+WFA^- cells (Figure 12A). No significant differences were observed in aspect ratio among the groups ($p > 0.9999$; Figure 12B), indicating that the cell elongation remained relatively consistent. In contrast, a modest but statistically significant difference in form factor (Figure 12C) was found between PV^-WFA^+ cells and PV^+WFA^- ($p = 0.0275$) and PV^+WFA^+ cells ($p = 0.0148$), indicating a higher cell shape complexity present in PV^-WFA^+ cells. Collectively, these results are in line with qualitative observations that WFA^+ PNNs that do not surround PV^+ cells tend to predominantly surround pyramidal cells.

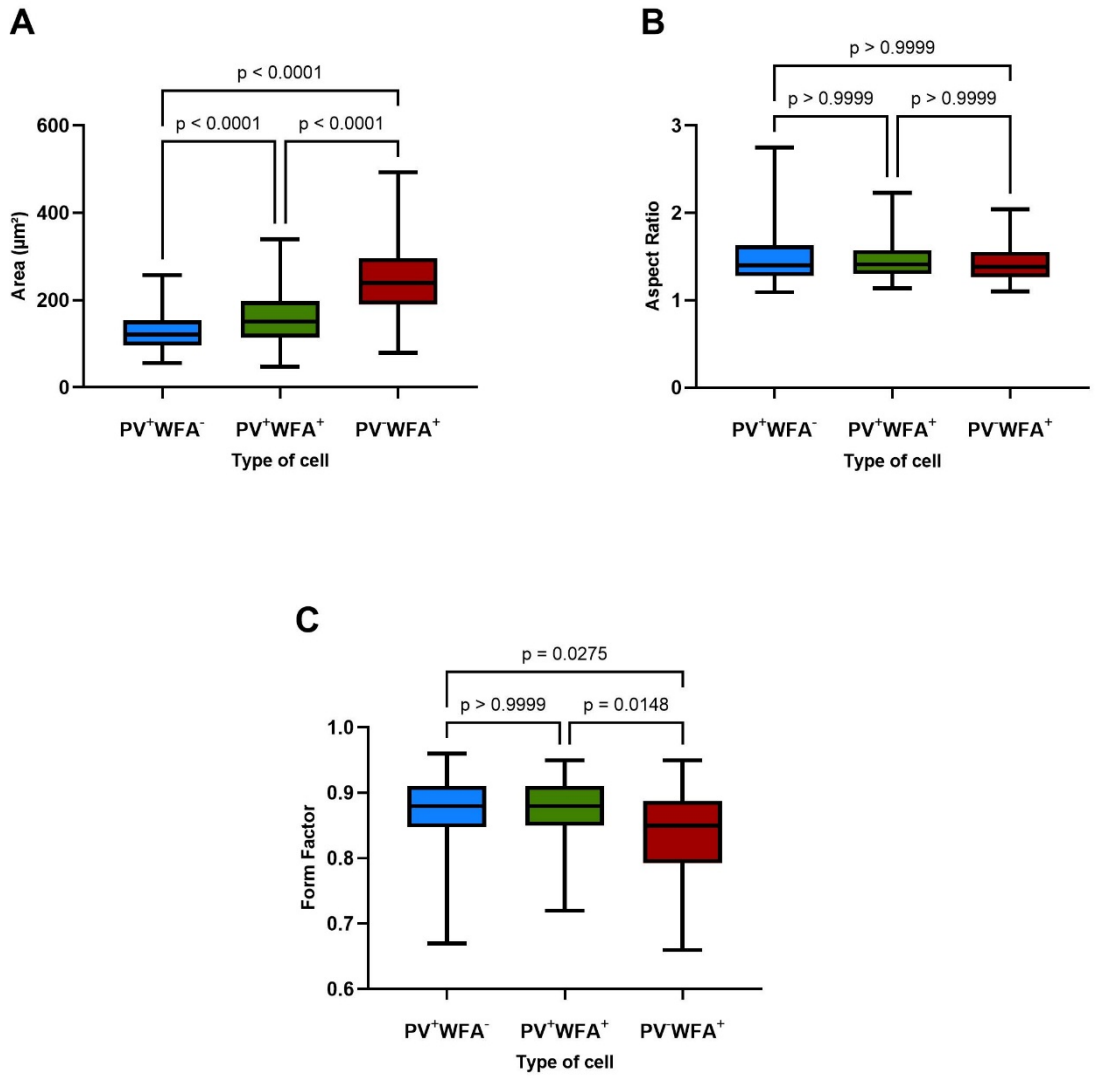

Figure 12. Comparison of morphometric parameters for $PV^{+}WFA^{-}$, $PV^{+}WFA^{+}$ and $PV^{+}WFA^{-}$ cells (combined data for BA10m and BA13b). Box plots show the comparisons for (**A**) soma area, (**B**) aspect ratio, and (**C**) form factor.

5. Discussion

This study investigated the proportion, laminar distribution and morphology of PNNs and GABAergic interneurons in BA10m and BA13b of the human cortex as well as the relationship between WFA^+ PNNs and PV^+ cells. The analysis revealed the following findings. Firstly, there were no statistically significant differences in the proportions or laminar distributions of PV^+ and CR^+ interneurons or WFA^+ PNNs between BA10m and BA13b. Secondly, interregional differences in the relative proportions of PV^+WFA^-, PV^+WFA^+ and PV^-WFA^+ cells were most pronounced in layers II and VI. Thirdly, morphological analysis of GABAergic interneurons indicated that PV^+ neurons were consistently larger than CR^+ neurons in both regions, with interneurons in BA13b showing greater morphological heterogeneity, particularly in cell elongation and soma complexity. Finally, morphological analysis of PV^+WFA^-, PV^+WFA^+ and PV^-WFA^+ cells confirmed differences in soma size and soma complexity between these cell groups.

The laminar distribution of PV^+ and CR^+ interneurons showed that layer IV had both the highest proportion and surface density of PV^+ cells in both BA10m and BA13b, consistent with previous findings that PV^+ interneurons are most predominant in the inner granular layer (Rudy *et al.*, 2011). The highest proportions of CR^+ cells were found in layers I, II and III aligning with studies indicating a predominance of CR^+ interneurons in supragranular layers (Gabbott *et al.*, 1997). The observed lack of significant differences in total PV^+ and CR^+ interneuron proportions between BA10m and BA13b is not necessarily surprising, since both cortical areas are located on adjacent sulci and separated only by BA14r. Interregional differences in the proportion of WFA^+ PNNs were also discrete, though BA13b showed a trend toward slightly higher proportions of WFA^+ PNNs in layers III, IV, and V. This could reflect a functional specialization of these layers, as PNNs are known to stabilize synaptic connections and regulate plasticity (Mauney *et al.*, 2013).

The most pronounced interregional differences in the relative proportions of PV^+WFA^-, PV^+WFA^+ and PV^-WFA^+ cells were observed in layers II and VI. Interregional differences were slightly less pronounced in layers III and V, and in layer IV the interregional difference was the most subtle. In addition, the relative proportion of PV+WFA+ cells was consistently higher in BA10m than in BA13b, potentially highlighting a region-specific enrichment of PV^+ interneurons surrounded by WFA^+ PNNs in BA10m. This may be related to the difference in regulation of the inhibitory microcircuitry in these cortical regions, since PNNs are involved in the regulation of synaptic plasticity and synaptic input of PV^+ interneurons (Carceller *et al.*, 2020). This finding is consistent with previous research showing that the biggest interregional difference in the relative proportions of the aforementioned cell types was found in layers II and VI (Banovac *et al.*, 2025).

Morphologically, the larger soma size of PV^+ cells compared to CR^+ cells in both regions corroborates previous findings that PV^+ interneurons, often basket or chandelier cells, have larger cell bodies than

CR^+ cells, which are predominantly (Rudy *et al.*, 2011). The significant differences in aspect ratio and form factor in BA13b, but not BA10m, suggests that BA13b may exhibit greater interneuron subtype diversity, potentially reflecting the functional differences between the two regions. The larger area of PV^-WFA^+ neurons compared to PV^+WFA^+ neurons in both regions is most likely related to the fact that most WFA^+ PNNs that do not surround PV^+ cells seem to be found surrounding pyramidal cells, which is in line with previous research (Enwright *et al.*, 2016).

This study also had several limitations. The research relied on postmortem human brain tissue, which can introduce potential variability due to factors such as fixation quality and postmortem interval). Nevertheless, the postmortem interval of all brain samples was between 6 and 11 h, which reduces the effect of postmortem tissue changes that become most prevalent after 24 h. Another limitation was that samples were acquired from male subjects, which is a consequence of the fact that the tissue was obtained from the Department of forensic medicine where most brain samples suitable for postmortem analysis were from male subjects. Even though the cortical regions analyzed in this research are not structurally different between male and female subjects, further research on female brain samples would still be needed in order to generalize these findings to the female population.

6. Conclusion

This study assessed the differences in proportion, laminar distribution, and colocalization of PNNs and GABAergic interneurons between BA10m and BA13b in the human orbitofrontal cortex. While no statistically significant differences between these two regions were found in overall proportions of PV^+ and CR^+ neurons, nor in the overall proportion of WFA^+ PNNs, layer-specific trends revealed more subtle differences between the regions. In BA13b, the proportion of WFA^+ PNNs among the total number of cells was higher in layers III, IV, and V. The relative proportions of PV^+WFA^-, PV^+WFA^+ and PV^-WFA^+ cells in layers II and VI were the most distinct in the two analyzed cortical regions, with layers III and V exhibiting less pronounced interregional differences. These findings suggest subtle region-specific roles for PNNs and GABAergic interneurons in modulating inhibitory control and synaptic plasticity.

The morphological distinctions, particularly the larger somatic size of PV^+ neurons and the region-specific shape differences in BA13b, further highlight functional specialization. These results are in line with the different roles of BA10m and BA13b. Future research should explore sex differences and include larger sample sizes to further elucidate the functional implications of these findings neuropathological conditions.

7. Acknowledgments

I would like to express my deepest gratitude to my mentor, Assistant Professor Ivan Banovac, MD, PhD for his invaluable guidance, expertise, and unwavering support throughout the course of this research.

8. Literature

1. Banovac, I. *et al.* (2019) 'Somato-dendritic morphology and axon origin site specify von Economo neurons as a subclass of modified pyramidal neurons in the human anterior cingulate cortex', *Journal of Anatomy*, 235(3), pp. 651–669. doi:10.1111/joa.13068.
2. Banovac, I. *et al.* (2022) 'The Distinct Characteristics of Somatostatin Neurons in the Human Brain', *Molecular Neurobiology*, 59(8), pp. 4953–4965. doi:10.1007/s12035-022-02892-6.
3. Banovac, I. *et al.* (2025) 'Morphological and Molecular Characteristics of Perineuronal Nets in the Human Prefrontal Cortex—A Possible Link to Microcircuitry Specialization', *Molecular Neurobiology*, 62(1), pp. 1094–1111. doi:10.1007/s12035-024-04306-1.
4. Betterle, C. and Zanchetta, R. (2012) 'The immunofluorescence techniques in the diagnosis of endocrine autoimmune diseases', *Auto-Immunity Highlights*, 3(2), pp. 67–78. doi:10.1007/s13317-012-0034-3.
5. Boenisch, T. (2005) 'Effect of heat-induced antigen retrieval following inconsistent formalin fixation', *Applied immunohistochemistry & molecular morphology: AIMM*, 13(3), pp. 283–286. doi:10.1097/01.0000146524.74402.a4.
6. Brodmann, K. (2005) *Brodmann's: Localisation in the Cerebral Cortex*. Translated by L.J. Garey. New York, NY: Springer.
7. Carceller, H. *et al.* (2020) 'Perineuronal Nets Regulate the Inhibitory Perisomatic Input onto Parvalbumin Interneurons and γ Activity in the Prefrontal Cortex', *The Journal of Neuroscience*, 40(26), pp. 5008–5018. doi:10.1523/JNEUROSCI.0291-20.2020.
8. Enwright, J.F. *et al.* (2016) 'Reduced Labeling of Parvalbumin Neurons and Perineuronal Nets in the Dorsolateral Prefrontal Cortex of Subjects with Schizophrenia', *Neuropsychopharmacology*, 41(9), pp. 2206–2214. doi:10.1038/npp.2016.24.
9. Fuster, J.M. (2015) The Prefrontal Cortex. 5th ed. Cambridge, MA: Academic Press.
10. Fuster, J.M. (1988) 'Prefrontal Cortex', in L.N. Irwin (ed.) *Comparative Neuroscience and Neurobiology*. Boston, MA: Birkhäuser, pp. 107–109. doi:10.1007/978-1-4899-6776-3_43.
11. Gabbott, P.L. *et al.* (1997) 'Local-circuit neurones in the medial prefrontal cortex (areas 25, 32 and 24b) in the rat: morphology and quantitative distribution', *The Journal of Comparative Neurology*, 377(4), pp. 465–499. doi:10.1002/(sici)1096-9861(19970127)377:4<465::aid-cne1>3.0.co;2-0.
12. Hathaway, W.R. and Newton, B.W. (2025) 'Neuroanatomy, Prefrontal Cortex', in *StatPearls*. Treasure Island (FL): StatPearls Publishing.
13. Judaš, M. *et al.* (2011) 'The Zagreb Collection of human brains: a unique, versatile, but underexploited resource for the neuroscience community', *Annals of the New York Academy of Sciences*, 1225 Suppl 1, pp. E105-130. doi:10.1111/j.1749-6632.2011.05993.x.
14. Karetko, M. and Skangiel-Kramska, J. (2009) 'Diverse functions of perineuronal nets', *Acta Neurobiologiae Experimentalis*, 69(4), pp. 564–577. doi:10.55782/ane-2009-1766.
15. Kostovic, I. *et al.* (1991) 'Zagreb research collection of human brains for developmental neurobiologists and clinical neuroscientists', *The International Journal of Developmental Biology*, 35(3), pp. 215–230.

16. Kringelbach, M.L. and Rolls, E.T. (2004) ‘The functional neuroanatomy of the human orbitofrontal cortex: evidence from neuroimaging and neuropsychology’, *Progress in Neurobiology*, 72(5), pp. 341–372. doi:10.1016/j.pneurobio.2004.03.006.

17. Kwok, J.C.F. *et al.* (2011) ‘Extracellular matrix and perineuronal nets in CNS repair’, *Developmental Neurobiology*, 71(11), pp. 1073–1089. doi:10.1002/dneu.20974.

18. Le Magueresse, C. and Monyer, H. (2013) ‘GABAergic Interneurons Shape the Functional Maturation of the Cortex’, *Neuron*, 77(3), pp. 388–405. doi:10.1016/j.neuron.2013.01.011.

19. Mauguière, F., Frot, M. and Isnard, J. (2008) ‘5.47 - Human Insular Recording and Stimulation’, in R.H. Masland et al. (eds) *The Senses: A Comprehensive Reference*. New York: Academic Press, pp. 707–716. doi:10.1016/B978-012370880-9.00190-0.

20. Mauney, S.A. *et al.* (2013) ‘Developmental Pattern of Perineuronal Nets in the Human Prefrontal Cortex and their Deficit in Schizophrenia’, *Biological psychiatry*, 74(6), pp. 427–435. doi:10.1016/j.biopsych.2013.05.007.

21. Mitchell, I.J. and Beech, A.R. (2011) ‘Towards a neurobiological model of offending’, *Clinical Psychology Review*, 31(5), pp. 872–882. doi:10.1016/j.cpr.2011.04.001.

22. Neumann, M. and Gabel, D. (2002) ‘Simple method for reduction of autofluorescence in fluorescence microscopy’, *The Journal of Histochemistry and Cytochemistry: Official Journal of the Histochemistry Society*, 50(3), pp. 437–439. doi:10.1177/002215540205000315.

23. Öngür, D., Ferry, A.T. and Price, J.L. (2003) ‘Architectonic subdivision of the human orbital and medial prefrontal cortex’, *Journal of Comparative Neurology*, 460(3), pp. 425–449. doi:10.1002/cne.10609.

24. Prkačin, M.V., Petanjek, Z. and Banovac, I. (2024) ‘A novel approach to cytoarchitectonics: developing an objective framework for the morphological analysis of the cerebral cortex’, *Frontiers in Neuroanatomy*, 18. doi:10.3389/fnana.2024.1441645.

25. Rudy, B. *et al.* (2011) ‘Three Groups of Interneurons Account for Nearly 100% of Neocortical GABAergic Neurons’, *Developmental neurobiology*, 71(1), pp. 45–61. doi:10.1002/dneu.20853.

26. Sadeghipour, A. and Babaheidarian, P. (2019) ‘Making Formalin-Fixed, Paraffin Embedded Blocks’, *Methods in Molecular Biology (Clifton, N.J.)*, 1897, pp. 253–268. doi:10.1007/978-1-4939-8935-5_22.

27. Sun, Y., Ip, P. and Chakrabartty, A. (2017) ‘Simple Elimination of Background Fluorescence in Formalin-Fixed Human Brain Tissue for Immunofluorescence Microscopy’, *Journal of Visualized Experiments: JoVE*, (127), p. 56188. doi:10.3791/56188.

28. Sy, J. and Ang, L.-C. (2019) ‘Microtomy: Cutting Formalin-Fixed, Paraffin-Embedded Sections’, *Methods in Molecular Biology (Clifton, N.J.)*, 1897, pp. 269–278. doi:10.1007/978-1-4939-8935-5_23.

29. Zaqout, S., Becker, L.-L. and Kaindl, A.M. (2020) ‘Immunofluorescence Staining of Paraffin Sections Step by Step’, *Frontiers in Neuroanatomy*, 14, p. 582218. doi:10.3389/fnana.2020.582218.

30. Zilles, K., Palomero-Gallagher, N. and Amunts, K. (2015) ‘Cytoarchitecture and Maps of the Human Cerebral Cortex’, in A.W. Toga (ed.) *Brain Mapping*. Waltham: Academic Press, pp. 115–135. doi:10.1016/B978-0-12-397025-1.00207-4.

9. Sažetak

Pia Kosanović

Povezanost perineuronskih mreža i GABA-ergičkih interneurona u orbito-frontalnoj moždanoj kori čovjeka

U ovom istraživanju ispitana je povezanost perineuronskih mreža (PNN) i GABA-ergičkih interneurona u ljudskoj moždanoj kori, s posebnim naglaskom na Brodmannova polja 10m i 13b. Imunohistokemijskim bojenjem i morfometrijskom analizom postmortalnog moždanog tkiva šest neurotipičnih odraslih osoba procijenjeni su udio, slojevita raspodjela i morfologija PV^+ i CR^+ interneurona te njihova povezanost s WFA^+ PNN-ovima.

Analizom nisu utvrđene statistički značajne razlike u ukupnoj gustoći PV^+ stanica, CR^+ stanica ili WFA^+ PNN-ova između analiziranih regija. Međutim, uočene su suptilne razlike u relativnim udjelima PV^+WFA^-, PV^+WFA^+ i PV^-WFA^+ stanica u pojedini slojevima moždane kore, pri čemu su slojevi II i VI pokazali najveće razlike među analiziranim regijama. Morfometrijska analiza pokazala je da PV^+ stanice imaju konzistentno veće površine tijela od CR^+ stanica, a interneuroni u Brodmannovom polju 13b općenito su imali morfološku raznolikost. PV^+WFA^+ stanice bile su značajno manje od PV^-WFA^+ stanica, što je u skladu s činjenicom da potonje većinom pripadaju populaciji piramidnih neurona.

Ovi rezultati ukazuju na regionalne specifičnosti u organizaciji inhibitornih kortikalnih krugova i sugeriraju ulogu PNN-ova u modulaciji strukturnih i funkcionalnih svojstava različitih podtipova interneurona. Dobiveni rezultati doprinose boljem razumijevanju inhibitornog ustroja ljudske moždane kore i mogu biti od koristi u translacijskim istraživanjima na neuropatološkom tkivu.

Ključne riječi: GABAergični neuroni, kalretinin, parvalbumin, perineuronske mreže, prefrontalni korteks

10. Summary

Pia Kosanović

The connection between perineuronal nets and GABAergic interneurons in the human orbito-frontal cortex

This study explored the relationship between perineuronal nets (PNNs) and GABAergic interneurons in the human cortex, focusing on Brodmann areas 10m and 13b. Using immunohistochemical labeling and morphometric analysis of postmortem tissue from six neurotypical adult brains, the proportion, laminar distribution, and morphology of PV^+ and CR^+ interneurons, and their association with WFA^+ PNNs were evaluated.

No significant interregional differences were found in the overall density of PV^+ cells, CR^+ cells, or WFA^+ PNNs. However, subtle layer-specific differences emerged in the relative proportions of PV^+WFA^-, PV^+WFA^+, and PV^-WFA^+ cells, with layers II and VI being the most distinct in each cortical area. Morphometric analysis revealed that PV^+ cells had consistently larger soma sizes than CR^+ neurons, and that interneurons in Brodmann area 13b displayed greater morphological heterogeneity. PV^+WFA^+ cells in both regions were significantly smaller than PV^-WFA^+ cells, consistent with the latter being predominantly pyramidal neurons.

These findings highlight region-specific patterns in inhibitory microcircuit organization and suggest a role for PNNs in modulating structural and functional properties of interneuron subtypes. The results advance understanding of inhibitory architecture in the human cortex and may inform translational studies involving neuropathological tissue.

Keywords: GABAergic interneurons, calretinin, parvalbumin, perineuronal nets, prefrontal cortex

11. Biography

I was born in May 1998 in Zagreb, Croatia. I completed my secondary education at Tituš Brezovački High School in Zagreb and spent one year as an exchange student at Bell High School in Ottawa, Canada. I am currently completing my final year of studies at the University of Zagreb, School of Medicine.

Throughout my academic journey, I have been actively involved in various extracurricular and scientific activities. I served as a class representative, mentored first year students, and worked as a student demonstrator at the Department of Internal medicine. In 2024, I was elected President of the Student section for infectious diseases and received the Dean's Award for my socially engaged work in the academic community.

In my final year, I began scientific research at the Croatian Institute for Brain Research, in the Laboratory for Immunohistochemistry, under the mentorship of Assistant Professor Ivan Banovac. I have authored and co-authored several case reports, presented at national and international medical congresses.

In addition to research and clinical interests I have volunteered for and participated in public health projects and student-led initiatives promoting mental health, patient education and international exchange. I am fluent in English (C1), have a basic knowledge of French (A2), and am currently studying Russian.